

28 July 2015

BACHELOR THESIS

# ON-LINE MONITORING OF MICROREACTOR PRODUCTS USING AN OPTOFLUIDIC MICROCHIP

Enzo Maikel Meijer

**Faculty of Science and Technology (TNW)  
BIOS Lab-on-a-Chip group**

Exam committee:  
prof. dr. J.G.E. Gardeniers  
dr. M. Odijk  
dr. ir. W. Olthuis  
F.T.G. van den Brink MSc  
F.H. Falke MSc

Student number:  
s0177466  
e.m.meijer@student.utwente.nl

### **Abstract**

Absorbance based measurements for the detection in microfluidic channels using an optical chip with embedded waveguides shows promise for use as a monitoring tool coupled on-line to an electrochemical cell. An experimental setup was build and tested for on-line monitoring of chemical reactions taking place in a microreactor chip using the optical sensing chip. With the chip measurements were performed alternating a flow of water and ruthenium tris-bipyridine, a chemical compound with a strong molar extinction coefficient. As a result of the signal instability quantitative analysis of the data could not be performed. Though a qualitative examination shows the system is capable of detecting different concentrations in the microfluidic channel. In order to implement the optical chip in the electrochemical setup, further research is needed.

# Contents

<b>Preface</b>	<b>5</b>
<b>1 Introduction</b>	<b>6</b>
1.1 Goals	6
1.2 Research Questions	7
1.3 Outline	7
<b>2 Theoretical Background</b>	<b>8</b>
2.1 Redox Reactions	8
2.1.1 Ruthenium tris-bipyridine	9
2.1.2 Potassium permanganate	9
2.2 Beer-Lambert Law	10
2.3 Evanescent Wave Spectroscopy	11
2.3.1 Fiber Optics	11
2.3.2 Evanescent Wave	12
<b>3 Experimental Part</b>	<b>13</b>
3.1 Reduction of $\text{KMnO}_4$	13
3.2 Calibration Measurements	13
3.3 Optofluidic Microchip	14
3.4 Experimental Setups	15
3.4.1 UV/vis Spectroscopy	15
3.4.2 Optical Sensing System	15
<b>4 Results and Discussion</b>	<b>17</b>
4.1 Reduction of $\text{KMnO}_4$	17
4.2 Calibration Measurements	18
4.3 Optical Chip Measurements	18
4.3.1 Ruthenium	18
4.3.2 Other Measurements and Discussion	20
<b>5 Conclusion &amp; Recommendations</b>	<b>22</b>
5.1 Conclusion	22
5.2 Recommendations	23

---

<b>Appendices</b>	<b>25</b>
<b>A Chemical reaction kinetics</b>	<b>26</b>
<b>B Oxidizing agents Ru(bpy)</b>	<b>28</b>
<b>C Calibration measurements <math>\text{KMnO}_4</math></b>	<b>29</b>
<b>D Additional Measurements</b>	<b>31</b>

# Preface

This report is the result of my bachelor assignment for Advanced Technology. From February till June 2015 I conducted a research on the implementation of an optofluidic microchip for on-line use in reaction monitoring. The research was done at the BIOS Lab-on-a-Chip group at the University of Twente.

I would like to thank Matieu Odijk, Assistant Professor at BIOS, for the opportunity to do this research and the valuable discussions during our meetings. Also, I would like to thank Floris van den Brink as my daily supervisor helping me with a great amount of things and good talks in between. Wouter Olthuis helped me structure my research questions and lent me one of his books. Thanks to Floris Falke of LioniX for providing the optofluidic microchip, the quick repair and the valuable insight he shared on the experimental setup. Henk van Wolferen and Hans de Boer assisted during the assembly of the setup. In addition, thanks to Harrie Waasdorp for designing the schematic overview of the setup. Last but not least, I would like to thank all the members and students of the BIOS group for the great time I had during this assignment. The open and friendly nature of the group makes it a really nice place to work.

# Chapter 1

## Introduction

This research will feature the characterization of an optical sensing chip to monitor chemical reactions in a Lab on a Chip. Currently BIOS is involved in a STW project (Stichting voor de Technische Wetenschappen) focusing on electrochemical conversions as a low-cost and fast method for drugs screening. The costs for developing new drugs has grown exponentially in the past few decades[1]. This creates a demand for a low-cost alternative drug screening method. Using electrochemical oxidation and chemical reactions of pharmaceuticals, certain metabolic pathways that occur in the body can be mimicked. This provides a tool that could accelerate *in vitro* tests for new potential drugs candidates. The goal of the project is to develop an electrochemical cell for on-line use with liquid chromatography and mass spectrometry. In 2012 Odijk et al.[2] developed an electrochemical cell in a lab on chip with improved conversion rates. The conversion efficiency study was performed by an optical flow-trough cell in combination with a spectrophotometer.

Since mass spectrometry is an expensive and relatively more complicated detection method , on-line analysis using the optical chip could provide a more straightforward alternative. Yue et al.[3] developed a microfluidic chip with embedded waveguides for detection in the evanescent wave field. This spectroscopy technique shows promise for on-line process analysis. LioniX BV has provided BIOS with the successor of this chip[4]. The optofluidic chip is specially designed for absorption based measurements in microfluidic channels. Fluid is transported through a microfluidic channel and brought in direct contact with a waveguide in which light is propagating, this area is called the sensing area. Here it is the evanescent field from the waveguide that interacts with the fluid.

### 1.1 Goals

The goal is to build and test an experimental setup for on-line monitoring of chemical reactions taking place in a microreactor chip using the optical sensing chip. This involves connecting the chip to both an optical and microfluidic path. Furthermore, to test the chip's functionality on chemical reactions, one or multiple suitable model reactions have to be determined. The characterization of the chip will include correlating the power output to the concentration present in the microfluidic channel. The measurements will be compared to those of a conventional UV/vis spectroscopy setup to determine the advantage of this novel sensing technique. Future goals of this project that are beyond the scope of this research, consists of implementing the chip in the electrochemical setup and a final aim is to embed the sensing waveguides directly into the electrochemical cell.

## 1.2 Research Questions

The outcome of the characterization will provide insight in the possibility of using the optofluidic micro chip as monitoring tool. Therefore the main research question is the following:

*Is it possible to use the optofluidic microchip as an online monitoring tool of microreactor products?*

In order to answer the main research question properly the following set of sub-questions were formulated.

- What is a suitable model reaction?
- What is the relation between the output power and analyte concentration in the chip (transfer function) and can we deduct the limit of detection and maximum concentration, given our model reaction?
- How do the measurements done with the optical chip compare to those of a conventional UV/vis spectroscopy set-up?

## 1.3 Outline

In this report first an overview of the required theory is given; the chemistry of oxidation-reduction reactions, theory on fiber optics and evanescent waves and finally the Beer-Lambert law, a fundamental equation for optical spectroscopy. The experimental section describes the calibration measurements, the optical sensing chip and both experimental setups. Next the results from the experiments are presented, the obtained data is interpreted and provided with a discussion. In the final chapter conclusions are drawn based on the research questions and recommendations are provided for future research.

# Chapter 2

## Theoretical Background

In the following chapter an overview is given of the theory applied for this research. First a section on the mechanics of redox reactions used in the model reactions that will be applied to test the chip. Next a section on fiber optic evanescent wave spectroscopy, explaining the propagation of light through an optical fiber and wave guide, together with the principle of the evanescent wave, which is responsible for the detection in the optofluidic chip. Lastly a section on the Beer-Lambert law correlating the measured absorbance to the concentration of the analyte. An chapter on chemical reaction kinetics can be found in [Appendix A](#).

### 2.1 Redox Reactions

Redox reaction are defined as all chemical reactions that include atoms that have their oxidation state changed. This involves the transfer of electrons between chemical species such as atoms, molecules or ions. The term redox is based on two types of electron transfer; reduction and oxidation:

**Reduction:** A *decrease* in the oxidation state by the *gain* of electrons.

**Oxidation:** An *increase* in the oxidation state by the *loss* of electrons.

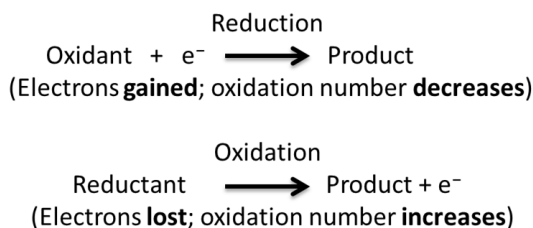


Figure 2.1: Reduction and oxidation reactions.

Redox reactions are always a matched set like acid-base reactions. During a reduction reaction an oxidation reaction is always taking place simultaneously. The partial reduction and oxidations reactions are called half-reactions. Each half-reaction has a standard electrode potential. This is based on the potential difference between half-reactions taking place at the cathode and the oxidation of hydrogen at the anode and is known as the standard hydrogen electrode (SHE). This standard electrode potential is denoted as  $E^0$  and measured in volt. In order for a

reduction reaction to proceed, an oxidant with a higher  $E^0$  than the reductant is needed. Similar, for an oxidation reaction to take place a reducing agent with a lower standard potential is needed, so that it can provide the electrons needed for the oxidant. Although, in practice not every combination of reductants and oxidants will provide a chemical reaction, since often an additional activation energy is involved.

In order to test the optical sensing chip for reaction monitoring, chemical model reactions have to be chosen. In the experimental setup a 488 nm laser will be used, therefore the choice of chemicals compounds are limited to those that show absorbance around this particular wavelength.

## 2.1 Ruthenium tris-bipyridine

Tris(bipyridine)ruthenium(II) chloride, Ru(bpy), is a bright red crystalline salt with the formula  $[\text{Ru}(\text{bpy})_3]\text{Cl}_2$ . It is the cation  $[\text{Ru}(\text{bpy})_3]^{2+}$  that has interesting optical properties. Ru(bpy) strongly absorbs light with  $\lambda_{\text{max}}$  of 452 nm and has a high molar extinction coefficient of  $14.600 \text{ M}^{-1} \text{ cm}^{-1}$ . [5]

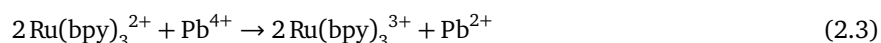
The redox reaction of interest is that of the 2+ to the 3+ complex.



This reaction has a standard electrode potential of 1.29V (vs. SHE)[5]. The focus is on a chemical conversion, an oxidizing agent with a higher potential is needed in order the reaction to take place. Literature mentions the chemical oxidation of Ru(bpy) using  $\text{PbO}_2$  [6][7].



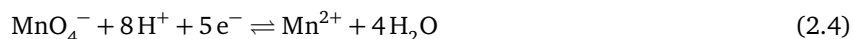
This reaction has a standard electrode potential of 1.61V[8]. Combining this with Ru(bpy) the total chemical reaction will become:



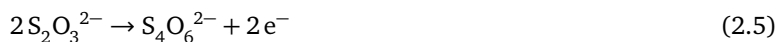
Furthermore based on standard electron potentials a reaction with silver (II) could also oxidise Ru(bpy) from the 2+ to the 3+ state. To reduction of  $\text{Ag}^{2+}$  to  $\text{Ag}^+$  has a standard electrode potential of 1.98V[8]. Due to limited time the reactions involving the chemical oxidation of Ru(bpy) by lead oxide or silver picolinate were not performed. A list of oxidizing agents for Ru(bpy) can be found in the appendix B.

## 2.1 Potassium permanganate

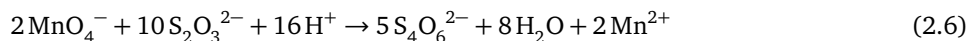
A second model reaction is the reduction of potassium permanganate. In an acidic solution, permanganate(VII) is reduced to the colourless 2+ oxidation state of the manganese(II)  $\text{Mn}^{2+}$  ion.  $\text{KMnO}_4$  has two absorption peaks at 526 nm and 546 nm with a molar extinction coefficients of respectively  $2.40 \cdot 10^3$  and  $2.38 \cdot 10^3 \text{ M}^{-1} \text{ cm}^{-1}$ .



This reduction has an  $E^0$  of 1.51V [8]. The oxidation of thiosulphate acts as a reducing agent with a standard electrode potential of 0.08V and the half reaction:



For the half reaction of  $\text{MnO}_4^-$  acidic conditions are needed, therefore  $\text{H}_2\text{SO}_4$  is added to the solution. Combined with the thiosulphate this gives the following redox reaction.



## 2.2 Beer-Lambert Law

Theory provided in the following section is based on the work 'Analytical Chemistry' [9]

The Beer-Lambert law makes it possible to correlate the amount of light absorbed to the concentration of substance present in the sample. In chemical analysis the law is commonly used for measurements.

Consider the radiation of a light source passing through a homogeneous substance in a sample, where  $I_0$  is the intensity of the source. Lambert found that the power of the transmitted radiation decreased exponentially with the path length  $b$  in centimetres, resulting in a reduced intensity of the transmitted radiation  $I_t$ :

$$T = \frac{I_t}{I_0} = 10^{-\alpha b} \quad (2.7)$$

In this equation the transmittance is called  $T$  and  $\alpha$  is a constant.

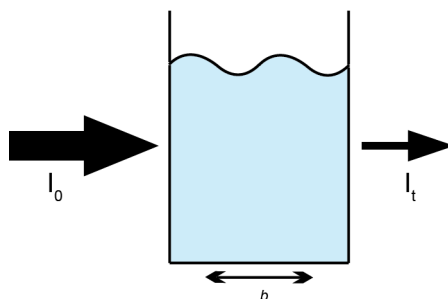


Figure 2.2: Absorbance of a homogeneous substance with incident radiation  $I_0$ , transmitted radiation  $I_t$  and path length  $b$ .

In 1852 German Physicist August Beer conducted a similar experiment in which he found a correlation between the absorbance of the transmitted radiation and the concentration of the substance. Resulting in a similar equation to that of the path length transmittance in equation (2.7)

$$T = \frac{I_t}{I_0} = 10^{-\beta c} \quad (2.8)$$

In which  $c$  is the concentration and  $\beta$  another constant. Combining the transmittance equations for both path length and concentration gives:

$$T = \frac{I}{I_0} = 10^{-\epsilon bc} \quad (2.9)$$

And put in logarithmic form:

$$\log T = \log \frac{I}{I_0} = -\epsilon bc \quad (2.10)$$

Here are  $\alpha$  and  $\beta$  combined into a new constant  $\epsilon$  called the molar absorptivity and has the units  $cm^{-1}mol^{-1}L$ . Now by changing the minus sign and taking the logarithm of the transmittance a new term is defined called the absorbance.

$$A = -\log T \quad (2.11)$$

And from here the Beer-Lambert law is defined as:

$$A = \epsilon bc \quad (2.12)$$

where  $A$  is the absorbance,  $b$  the path length in cm and the constant  $\epsilon$  the molar absorptivity in  $cm^{-1}mol^{-1}L$ . With a fixed path length and molar absorptivity, the concentration in the sample can be determined based on the transmittance obtained by a sensor like a spectrometer or a photodiode.

## 2.3 Evanescent Wave Spectroscopy

*Theory provided in the following section is based on the work of [10] [3] [11].*

Fiber optic evanescent wave spectroscopy is a specific application of UV/vis spectroscopy in which waveguides in combination with a microfluidic channel are used instead of a conventional sample cell.

### 2.3 Fiber Optics

An optical fiber functions as a waveguide and can be used to transmit light over a certain distance. The fiber consists of a transparent core surrounded by a cladding, both made of a dielectric material. The light in the fiber is transmitted along its axis by the process of total internal reflection. Here the refractive index of the cladding has to be higher than the core. When the incident beam of light in the core strikes at the boundary of the cladding with an angle greater than the critical angle, the light is completely reflected. The light bounces between the boundary of the core and the cladding and is confined in the optical fiber.

### 2.3 Evanescent Wave

Alongside the total reflection of the light beam within the waveguide an evanescent wave develops right at the boundary of the core and cladding. Since electromagnetic waves cannot be discontinuous at a boundary, a portion of the wave continues outside of the boundary, in this case the dielectric cladding. The amplitude of the evanescent wave decreases exponentially with the distance from the core surface and the wave practically vanishes at a distance called the depth of penetration. The depth of penetration of the evanescent wave outside the core is in the order of a few microns and depends on the wavelength of the beam, the incident angle and both refractive indices of the optical fiber and the cladding. Furthermore by increasing the mode number the evanescent wave will penetrate further in the outer layer.

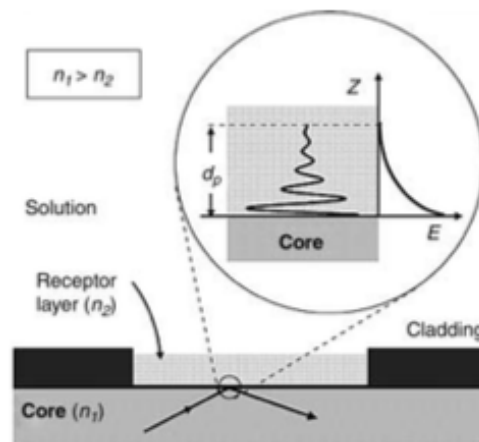


Figure 2.3: The evanescent wave at the core surface with refractive indices  $n_1 > n_2$ . Magnification: exponential decay of the evanescent wave and depth of penetration  $d_p$ . Figure adapted from *Chemical Sensors and Biosensors*[11].

It is the evanescent wave that will interact with the analyte in the optical chip. Whereas normally this wave would travel through the dielectric material. Now, on a small area on the chip in the absence of cladding, the core from the optical fiber is in direct contact with the microfluidic channel. This enables the evanescent wave to reach the fluid in the channel and interact with the molecules in the solution. Absorption can take place and then the remaining part of the evanescent wave will travel back in to the waveguide. Now this transmitted wave can be measured using a sensor and ultimately related to the concentration.

# Chapter 3

## Experimental Part

### 3.1 Reduction of $\text{KMnO}_4$

For the reduction reaction a stock solution was prepared of 1 mM  $\text{KMnO}_4$  and 10 mM  $\text{H}_2\text{SO}_4$  was added to create an acidic solution. The solution was distributed in 1 ml, 1 cm cuvettes which were put in a UV/vis spectrometer. The reduction reaction stated in 2.4 was tested by the addition of a 100 mM solution  $\text{S}_2\text{O}_3^{2-}$  creating the redox reaction of 2.6 Small amounts of  $\text{S}_2\text{O}_3^{2-}$  were added to the cuvette using a pipette and ranged from 10 to 100  $\mu\text{L}$ .

### 3.2 Calibration Measurements

In the UV/vis spectrometer calibration measurements were performed for both ruthenium bipyridine and potassium permanganate. By setting up a calibration curve an unknown concentration of the analyte can be determined by comparing the result to a set of known concentrations. Table 3.1 shows Ru(bpy) concentrations prepared in the the seven cuvettes prepared for the experiment. The solutions were prepared from a 61.7  $\mu\text{M}$  stock solution  $[\text{Ru}(\text{bpy})_3]\text{Cl}_2$ . The cuvettes were placed in UV/vis spectrometer and the absorbance was measured at  $\lambda_{max}$  452 and at 488 nm, the wavelength of the laser that will be used in subsequent experiments.

Cuvette	Concentration in $\mu\text{M}$
1	61.7
2	30.9
3	15.4
4	6.17
5	3.09
6	1.54
7	0.61

Table 3.1: Overview of the concentrations Ru(bpy) for the calibration measurement.

### 3.3 Optofluidic Microchip

LioniX has provided BIOS with the optofluidic microchip, this chip uses embedded optical waveguides for absorption based measurements in a microfluidic channel. Fluid transported through the channel is brought into contact with a waveguide through which light propagates. In the sensing area the protective oxide above the waveguide is removed, this allows the evanescent wave to be in direct contact with the fluid and absorption can take place. The optofluidic chip features two separate microfluidic channels with a length of 26 mm and cross-section of  $300 \times 100 \mu\text{m}$ . Both channels are equipped with a sensing area of 1 mm and 5 mm.

In figure 3.1a on the right hand side of the chip the input and outputs of the waveguides are shown. Starting at the upper waveguide, this is the input of the chip and the optical signal is split. One part will travel through the 1 mm sensing area and the other one is directly coupled back as a reference channel. Output 1 is the reference channel and output 2 the sensing channel which interacts with the fluid. For the 5 mm sensing area the fiber array has a similar configuration

The chip is designed for wavelengths between 488 and 635 nm, which is compatible with the 488 nm laser used in the experimental setup. Wavelengths outside the this region can be used, but a higher noise level or loss of signal is expected.

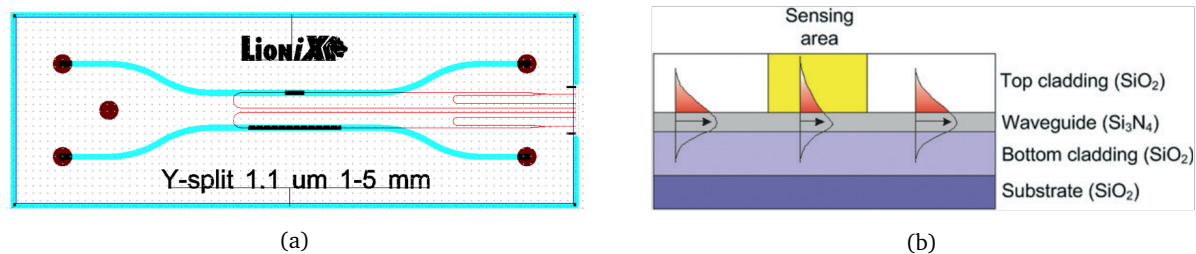


Figure 3.1: **(a)** Layout of the optofluidic microchip. Two separate microfluidic channels are shown with in and outlets on the side, on the right hand side the fiber array is visible. The 1 mm and 5 mm sensing areas are shown as the black areas in the middle. **(b)** Schematic cross-section of the chip with the evanescent wave probing the sensing area.

### 3.4 Experimental Setups

In the next section an overview of the experimental setups is given. The UV/vis spectroscopy setup is for initial experiments on the model reactions and calibration measurements. The optical sensing system was built for performing measurements using the optofluidic chip in combination with a microreactor.

#### 3.4 UV/vis Spectroscopy

The initial experiments for testing the model reactions are performed using a conventional UV/vis spectroscopy setup. The light source, a deuterium lamp, provides a continuous spectrum which is used for spectral and absorbance measurements of the analyte. The light from the source is coupled in an optical fiber which then passes through a 1 cm disposable cuvette. Here in the fluid absorbance takes place and then the transmitted beam is passed into another optical fiber connected to a Maya 2000PRO spectrophotometer. The spectrometer is connected to a laptop and data is processed by Labview. A dark signal without light together with a reference signal from the light source without analyte are measured. Both the signal of the measurement and the reference are subtracted by dark signal. After this correction the signal is divided by the reference to obtain the transmittance, from here the absorbance can be calculated using equation 2.11

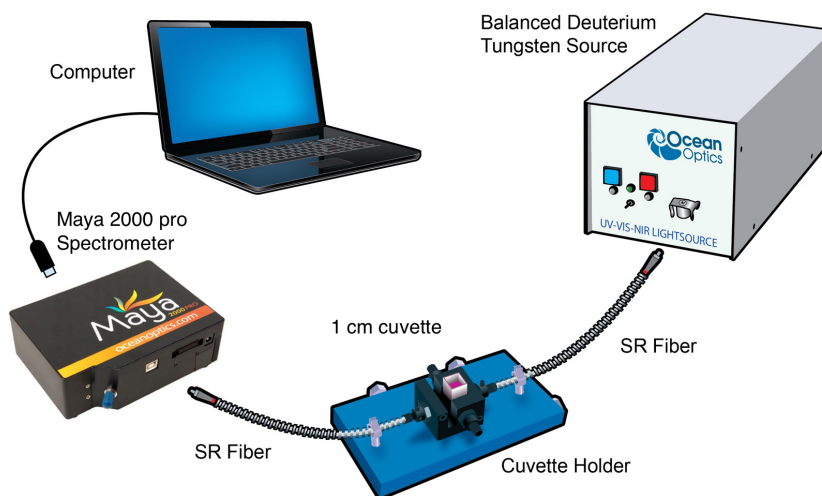


Figure 3.2: Overview of the UV/vis spectroscopy setup.

#### 3.4 Optical Sensing System

In order to do measurements using the optofluidic chip, a new experimental setup was build. The experimental setup consists of a microfluidic and optical path which interacts with each other in the optofluidic microchip

The microfluidic path starts with two Nemesys pumps loaded with two glass syringes. Typical flow rates varied between  $1 \mu\text{L}/\text{min}$  to  $14 \mu\text{L}/\text{min}$ . Via glass capillaries the fluids from the pumps are transferred to a Micronit microreactor, type R150.332 with an internal volume of  $6 \mu\text{L}$ , in which two analytes are mixed together. From here the fluid flows through the optical chip where it is brought in contact with the evanescent wave, then the

analyte leaves the chip and is collected in a glass vial as waste. In the optical chip the microfluidic channel with the 1 mm sensing area is used. The microreactor can be used to mix two substances for chemical reactions, but also for uncomplicated switching between flows of a single fluid. By alternating the pumps a segmented flow of water and analyte can be created.

At the source for the optical path there is a Coherent Sapphire laser with an output wavelength of 488 nm. The laser is coupled into an optical fiber through a Newport single mode fiber coupler which is connected to the optical fiber of the chip using a mating sleeve. This allows simple switching between optical fibers without repeatedly coupling the laser beam in the optical fiber. From the input channel the light propagates through the optical chip where absorption can take place. There it passes into another fiber for the output which is connected to a photodiode power sensor. The S150C power meter from Thorlabs measures the output power from the optical chip in watt and is connected to a laptop via an usb-interface, here the data is processed by software from Thorlabs. Finally a case with protective glass is placed over the optofluidic chip to block stray light from the chip.

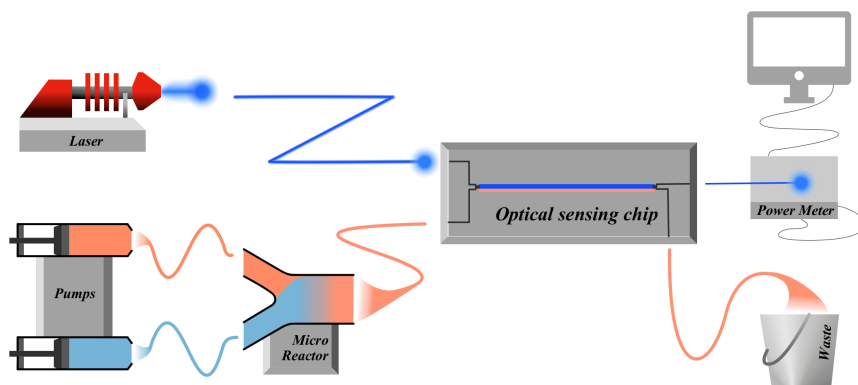


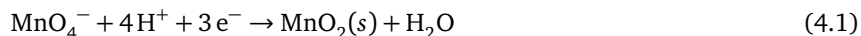
Figure 3.3: Schematic overview of the optical sensing system with the optical (blue) and microfluidic (orange) paths and the optofluidic chip at the centre.

# Chapter 4

## Results and Discussion

### 4.1 Reduction of $\text{KMnO}_4$

The chemical reaction of  $\text{KMnO}_4$  reduced by thiosulphate showed promise use, the magenta colour disappeared quickly by the addition of thiosulphate, resulting in a colourless substance. Later it was found, that when smaller amounts of 10 to 20  $\mu\text{L}$ , of  $\text{NaS}_3\text{O}_3$  were added to the solution another reaction takes place in which a brown suspension is formed as is shown in figure 4.1. This is the formation of Manganese(IV) oxide,  $\text{MnO}_2$ , with the following half-reaction:



This reaction usually occurs if the solution is not acidic enough, but with 10 mM  $\text{H}_2\text{SO}_4$  this is not expected. Here the cause is a shortage of  $\text{NaS}_3\text{O}_3$  as reducing agent changing the  $\text{MnO}_4^-$  to  $\text{MnO}_2(\text{s})$  instead of  $\text{Mn}^{2+}$ . The addition of more thiosulphate will prevent this unwanted reaction from taking place. Adding 10  $\mu\text{L}$   $\text{NaS}_3\text{O}_3$  to the  $\text{KMnO}_4$  results in a mole ratio of 1:1, whereas the total redox reaction (2.6) states a 1:5 ratio.

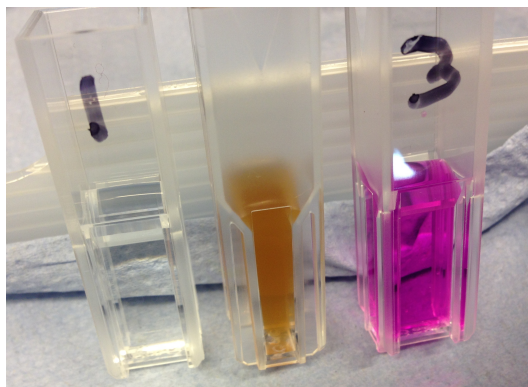


Figure 4.1: Three cuvettes **Left:** Colourless solution after adding 50  $\mu\text{L}$   $\text{NaS}_3\text{O}_3$  **Middle:** Brown suspension with  $\text{MnO}_2(\text{s})$ . **Right:** Stock solution  $\text{KMnO}_4$ .

Since the characterization of the chip involves the measurement of low concentrations in the chip, the formation of the solid particles is not desirable for they can influence the signal or possibly even block the channels or tubing.

For this reason no reactions with potassium permanganate were used in the optical chip. It is possible that another reaction involving reduction  $\text{MnO}_4^-$  might prevent the formation of  $\text{MnO}_2$ .

## 4.2 Calibration Measurements

Table 4.1 shows Ru(bpy) concentrations in the seven cuvettes prepared for the experiment. The solutions were prepared from a  $61.7 \mu\text{M}$  stock solution  $[\text{Ru}(\text{bpy})_3]\text{Cl}_2$ . The cuvettes were placed in UV/vis spectrometer and the absorbance was measured at  $\lambda_{\text{max}}$  452 nm and the wavelength of the laser that will be used in subsequent experiments (488 nm).

Cuvette	Concentration in [ $\mu\text{M}$ ]	Absorbance at 452 nm	Absorbance at 488 nm
1	61.7	09.861	0.1586
2	30.9	0.4300	0.0775
3	15.4	0.2152	0.0398
4	6.17	0.0876	0.0165
5	3.09	0.0446	0.0087
6	1.54	0.0221	0.0037
7	0.61	0.0108	0.0028

Table 4.1: Overview of the concentrations Ru(bpy) in the 1 ml, 1 cm cuvettes with the corresponding absorbance (arbitrary units) measured in the spectrometer at 452 and 488 nm.

In figure 4.2a the absorbance as a function of time is shown. The value for the absorbance is obtained by taking the mean absorbance during the time of the cuvette in the spectrometer. Next the absorbance is plotted versus the concentration of the solution and a linear fit is obtained by using the MATLAB polyfit function. This is shown in figure 4.2b. The datafit provides a linear coefficient of  $13.9 \text{ A mM}^{-1}$ . This value can be attributed as the molar extinction coefficient  $\epsilon$  in the Beer-Lambert law in equation 2.12. This value corresponds with the one found in literature of  $14.6 \text{ mM}^{-1} \text{ cm}^{-1}$  [5]. To determine the validity of the calibration curve, analysis of the linear regression is done by calculating  $R^2$ , the coefficient of determination. Here  $R^2 = 0.9999917$ .

Another calibration curve was established for the absorbance at the wavelength of 488 nm. Here a linear coefficient of  $2.55 \text{ A mM}^{-1}$  was found with  $R^2 = 0.99977$ . At the lowest concentration of  $0.61 \mu\text{M}$  an absorbance of 0.0028 was measured, a distinction between signal and baseline was clearly visible and the limit of detection was not yet reached.

Calibration measurements for the potassium permanganate were done as well. These can be found in Appendix C.

## 4.3 Optical Chip Measurements

### 4.3 Ruthenium

The experiments on chemical oxidation or reduction of the model reactions did not yield the anticipated results. Therefore the choice was made to measure the absorbance of Ru(bpy) in aqueous solution. Figure 4.3 shows output power of the optical chip by alternating between water and Ru(bpy) every two minutes keeping a constant

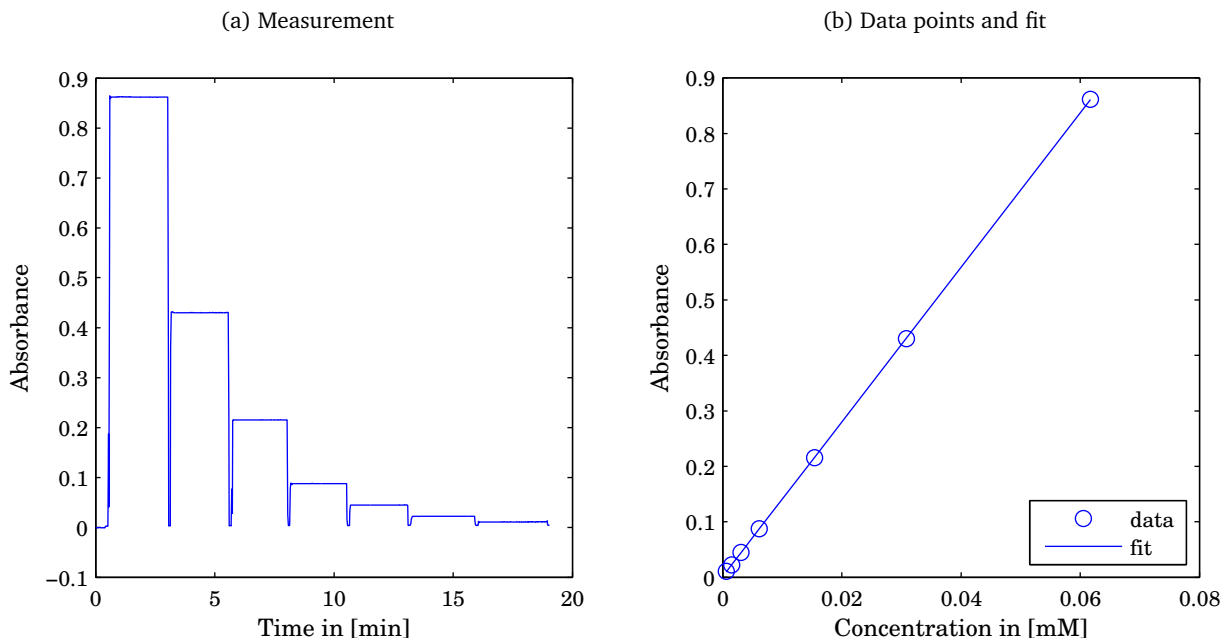


Figure 4.2: Calibration measurement for  $\text{KMnO}_4$  at the wavelength of 452 nm. 4.2a shows the absorbance over time for the seven prepared solutions. 4.2b shows the obtained data points together with the datafit, a linear coefficient of  $13.9 \text{ A mM}^{-1}$  with  $R^2 = 0.9999917$ .

flow rate of  $12 \mu\text{L}/\text{min}$ . When the pump is switched to Ru(bpy) it takes about 25 seconds before the fluid reaches the sensing area, then the signal rapidly decreases to 300 nW and reaches a final value around 292 nW. When the pump is switched back to water the signal increases but not nearly as fast as the decreasing signal, after two minutes it reaches 422 nW. Ru(bpy) is again introduced at the 6 minute mark and rapid decline towards 297 nW is visible and afterwards this process repeats one more time and ends with the pump switched back to water.

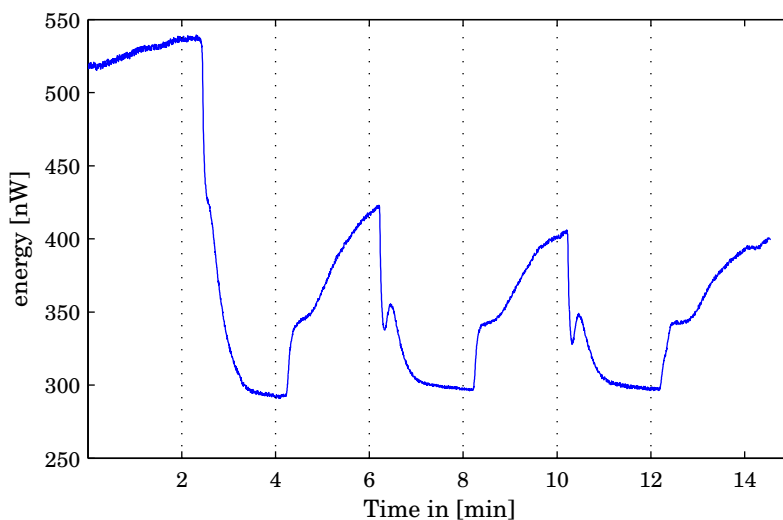


Figure 4.3: Alternating  $\text{H}_2\text{O}$  and Ru(bpy) with an interval of 2 minutes at a flow rate of  $12 \mu\text{L}/\text{min}$ , the dashed lines indicate switching of the pumps.

It takes a longer time to get the signal back to the initial value while on the other hand when Ru(bpy) is introduced to the system it immediately responds with a rapid signal change. This leads to the shark fin shapes as seen in figure 4.3. Apparently Ru(bpy) remains in the microfluidic channel (or only the sensing area) and it takes up to 10 to 15 minutes of flushing in order to get the original signal back. A possible explanation might be that Ru(bpy) somehow tends to 'stick' to the SiO<sub>2</sub> surface of the channel or the Si<sub>3</sub>N<sub>4</sub> surface of the sensing area. Binding of the Ru(bpy) molecules to silicon nitride surface can change the absorbance in the evanescent wave as well as the refractive index of the silicon nitride, causing a change in signal.

The binding of the Ru(bpy) to the Si<sub>3</sub>N<sub>4</sub> surface in the presence of an evanescent wave shows resemblance to that of Surface Plasma Resonance (SPR)[12]. Here surface plasmons are excited under the influence of an incident light wave. At the critical angle, or SPR angle, there is maximum loss of the reflected light intensity. The SPR Angle is dependent on the optical properties of the system, in this case the refractive indices on both sides of waveguide. Now when Ru(bpy) binds to the surface the critical angle changes as result of a different refractive index and this is shown in the output power of the chip. SPR and the binding constant also could explain the shark fin shapes found for the different response when water or Ru(bpy) is introduced into the system. The binding constant describes the affinity of the ligands and is denoted as the association rate divided by the dissociation rate. Ru(bpy) binds easily to silicon nitride corresponding with a quick signal change, indicating a high association constant. A low dissociation constant translates to the long period need the flush the channel in order to reach the initial signal.

When Ru(bpy) is passing the sensing area and the signal decreases there is also a small oscillation visible around 350 nW. At this moment there is no clear explanation for this fluctuation. It could be an effect of the Ru(bpy) binding to the surface as mentioned above. Furthermore, a great change in flow rates is not expected since the pumps are switched on and off simultaneously. By mixing the water flow to Ru(bpy) in microreactor pressure fluctuations upon switching of the pumps could possibly give rise to these fluctuations in concentrations.

Similar measurements were conducted at different flow rates between 4 and 20  $\mu\text{L}/\text{min}$  with comparable results. A quick response to Ru(bpy) and no full return to the original signal without a long time of cleaning the chip with water. The first measurement described above shows the most clear results but at other flow rates the shark fins and oscillation in the middle were found as well showing no clear dependency on the flow rates. Figures of the other experiments can be found in Appendix D. The data shows that a distinction between Ru(bpy) and water is possible. Values for Ru(bpy) varied between 282 nW and 307 nW, for water the signal range was wider varying between 508 nW and 556 nW. Therefore it is not possible to perform a quantitative analysis, relating the output power to the concentration of the analyte.

### 4.3 Other Measurements and Discussion

After a couple measurements with water and Ru(bpy) the system was flushed and then rested for 45 minutes. Afterwards water was flushed again and suddenly a great decrease in signal was measured, as is shown in figure 4.4. The signal starts at 507 nW then rapidly drops to 24 nW and over the course of 3 minutes it climbs back to the initial value. In the end the output signal for water is even higher, around 548 nW.

An explanation for the sudden decrease supports the idea that part of the Ru(bpy) binds to the channel wall or waveguide. Because of the laminar flow rate in the channel the flow speed at the wall is almost zero. When water is flushed not all Ru(bpy) is cleaned due to low flow rate at the wall. When the system is in rest diffusion takes place and the Ru(bpy) has a chance to dissociate. Afterwards when the pump is turned on the remaining Ru(bpy) dissolved and passes the sensing window, causing a dip in the signal. In this experiment the signal drastically drops

to 24 nW, much lower compared to the normal flow of Ru(bpy). Here it could also be possible that the sensing area in the channel functions as a small gutter in which compounds can accumulate before they are flushed out. The absence of SiO<sub>2</sub> cladding in the sensing area changes the dimensions of the microfluidic channel there could be a change in the flow profile at this particular area. Further research using a COMSOL model could provide more insight in the flow profile of the sensing area and its effects. The measured signal of 24 nW indicates the sensing range is lower than was measured in previous experiments suggesting the optical sensing chip is capable of detecting higher concentrations.

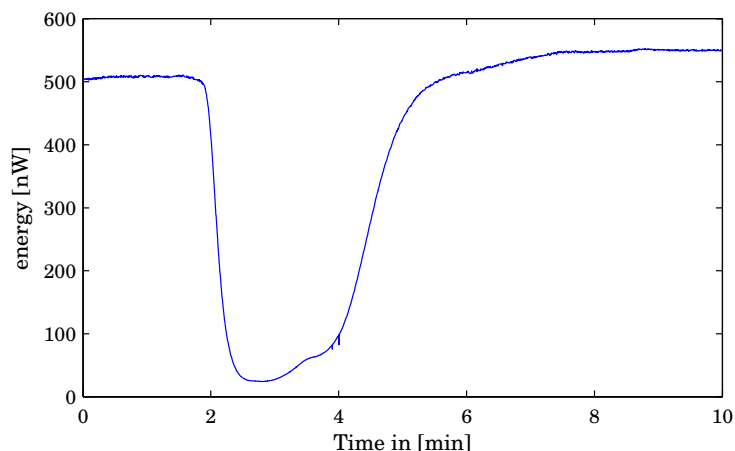


Figure 4.4: Considerable signal decrease after the chip rested for 45 minutes then pump with water was switched back on.

During the initial tests of the optical setup, strong fluctuations in the signal were found. Without a stable signal it was not possible to distinguish between a difference in absorbance and drift on the signal. Furthermore external factors played a great role in the stability of the signal. Other light sources especially a halogen desk lamp contributed heavily on the instability of the signal, even with the protective casing filtering out UV light. This indicates a possible temperature dependency in the system. Later on when the laser was once again coupled into the optical fiber it was found that the cylindrical angle in which the fiber is placed in the optical fiber coupler plays an important role. Light from the laser source is polarized and when the optical fiber is coupled it should be placed in the same angle as the polarization angle in order to maintain a stable signal throughout the optical fiber and chip. When this was discovered a great increase in signal stability was found.

Both sensing windows on the LiniX chip feature a reference and a sensing channel. During the experiments only the signal from the sensing channel was used. Later on LiniX provided us with another power meter and usb-interface which allows for simultaneous measurements on both channels. This can lead to a higher accuracy of the measurement, fluctuations present both the sensing and reference channel can be cancelled out. Though due to limitations in the software and time experiments with a reference channel were not performed. Furthermore the addition of the reference channel is yet in an experimental phase, the split in the optical path can deviate from a 50/50 split. Also a difference in signal can arise since the reference channel has a different path length together with the absence of a sensing window.

# Chapter 5

## Conclusion & Recommendations

### 5.1 Conclusion

For this research a new experimental setup was built to perform measurements with the optical sensing chip to detect concentrations in a microfluidic channel. Different model reactions were examined and a calibration curve for Ru(bpy) was made. In the optical setup several measurements with alternating a flow between water and Ru(bpy) were carried out. Based on the experimental results the conclusions will be drawn according to the main research question and sub-questions stated in chapter 1.

*What is a suitable model reaction?*

For this experimental setup a chemical compound must show absorbance at a wavelength equal or close to the operating wavelength of the laser, here this is 488 nm. Then by a chemical reaction this absorbing compound needs to be either formed or disappear without the formation of unwanted side products. The reduction reaction of  $\text{KMnO}_4$  in this form did not meet these requirements because  $\text{MnO}_2(\text{s})$  was formed. Possibly another reaction involving potassium permanganate might resolve this issue.

The strong optical properties of Ru(bpy) are useful and the chemical oxidation using lead oxide or silver picolinate need to be further investigated. In the optical chip a quick response to Ru(bpy) was found but afterwards thorough flushing of the system was needed. If the Ru(bpy) binds to the  $\text{SiO}_2$  channel wall or  $\text{Si}_3\text{N}_4$  waveguide, this might explain the behaviour of the optical chip, with the observed shark fin curves as a result of the association and dissociation constants. If this binding occurs an interesting surface property of Ru(bpy) is found, which can be further researched. But because of the low dissociation constant another model reaction might be preferred for the characterization of the chip.

*What is the relation between the output power and concentration of the chip (transfer function) and can we deduce the limit of detection and maximum concentration, given our model reaction?*

With the optical chip a difference in output signal was measured based on a variation in concentration. Over the course of the experiments values for 61.7  $\mu\text{M}$  solution Ru(bpy) varied between 282 nW and 307 nW. For  $\text{H}_2\text{O}$  initial values varied between 508 nW and 556 nW. These values show that a qualitative distinction between analytes can be made. Because of the variance in the signals an accurate quantitative analysis is not possible.

Therefore a transfer function can not be given at this point. But based on the data it is suggested that detection lower concentrations surely can be done. The found output value of 25 nW indicates the optical chip is capable of handling much higher concentrations as well but further testing is needed.

The cause for the fluctuations in a decreasing signal are still unclear. For determining a concentration, the final value in which the system reaches a steady state is the value of interest. Then a fluctuation during the settling time is not important. Though when one is interested in the detection of short living compounds, these fluctuations might interfere.

*How do the measurements of the optical chip compare to those of a conventional UV/vis spectroscopy set-up?*

Since a reliable quantitative analyses of the measurements was not possible, a good comparison between of the optical chip and the conventional UV/vis spectroscopy set-up can not be provided. For now a conventional set-up gives a more accurate and steady signal.

*Is it possible to use the optofluidic microchip as an on-line monitoring tool of microreactor products?*

The obtained data indicates it is possible to detect concentrations in a microfluidic channel and this is supported by the literature in which promising results were found using a similar optical chip [4]. However in the current experimental setup quantitative analysis of chemical compounds is not yet possible due to the instability of the signal. In addition, the slow dissociation of Ru(bpy) withholds the system from doing consecutive measurements. For the future goal of implementing the optical sensing chip in an electrochemical setup for on-line drugs screening, further research is needed.

## 5.2 Recommendations

- Further exploration of the reducing reactions of  $\text{KMnO}_4$  in order to find a more suitable model reaction.
- A closer analysis of the possible surface binding of Ru(bpy) associated with SPR and change in refractive indices.
- Implementation of the reference channel in the measurements. A second power meter and interface are available but need to be set up in the software (Thorlabs or Labview). This provides a more steady signal for measurements.
- Measurements on both the 1 mm and 5 mm sensing area and comparison of the results.
- Quantitative analysis, testing the chip at different concentrations in order to formulate the transfer function and deduce the limit of detection and maximum concentration, given the model reaction.
- Based on the above item, compare the results to conventional UV/vis spectroscopy set-up.
- Incorporation of a multi-wavelength light source. Xio Photonics, in cooperation with LioniX, has developed a multi-source light with three (to eight) lasers with different wavelengths. This allows detection of multiple compounds with different absorbance spectra.

# Bibliography

- [1] B. Munos. Lessons from 60 years of pharmaceutical innovation. *Nature Reviews Drug Discovery*, 8:959–968, 2009.
- [2] Mathieu Odijk, Wouter Olthuis, A. van den Berg, Liang Qiao, and Hubert Girault. Improved conversion rates in drug screening applications using miniaturized electrochemical cells with frit channels. *Analytical Chemistry*, 84(21):9176–9183, 2012.
- [3] Jun Yue, Floris H. Falke, Jaap C. Schoutena, and T. Alexander Nijhuis. Microreactors with integrated uv/vis spectroscopic detection for online process analysis under segmented flow. *Lab Chip*, 13:4855–4863, 2013.
- [4] F. Falke. *Sensing chip for integrated absorption spectroscopy using evanescent field sensing*. LioniX BV, 2015.
- [5] K. Kalyanasundaram. Photophysics, photochemistry and solar energy conversion with tris(bipyridyl)ruthenium(ii) and its analogues. *Coordination Chemistry Reviews*, 46:159–242, 1982.
- [6] Neil W. Barnett, Tim a. Bowser, and Richard a. Russell. Determination of oxalate in alumina process liquors by ion chromatography with post column chemiluminescence detection. *Analytical Proceedings including Analytical Communications*, 32(2):57, 1995.
- [7] Toshiyuki Abe, Yukari Tamada, Hidenobu Shiroishi, Mieko Nukaga, and Masao Kaneko. Catalytic water oxidation using chemically generated. pages 389–395, 1999.
- [8] A. J. Bard, R. Parsons, and J Jordan. *Standard Potentials in Aqueous Solutions*. Marcel Dekker, New York, 1985.
- [9] Gary D. Christian. *Analytical Chemistry, 7th Edition*. Wiley and Sons, 2013. 978-0-470-88757-8.
- [10] R.M. de Ridder. *Optical basic functions and microsystems*. 2012.
- [11] Florinel-Gabriel Banica. *Chemical Sensors and Biosensors Chemical Sensors and Biosensors*. Wiley, 2012.
- [12] Anna J Tudos and Richard B M Schasfoort. Introduction to Surface Plasmon Resonance. pages 1–15, 2008.

# Appendices

# Appendix A

## Chemical reaction kinetics

Theory provided in the following section is based on the work 'Analytical Chemistry' [9]

Chemical kinetics describes at which rate chemical reactions take place and the conditions which can influence the speed of such a reaction. The order of the reaction is defined as the extent to which the reaction rate depends on the concentration of the reacting substances. The following reaction is considered a first order reaction.



It is a reaction in which a single substance A is decomposing to one or more different products P. The rate of the disappearance of A is equal to the rate the reaction and is proportional to the concentration of A. This relation can be put in differential form and is known as the first-order rate law.

$$-\frac{dA}{dt} = k[A] \quad (\text{A.2})$$

Here  $k$  is the specific rate constant, specified at a certain temperature. The dimensions of  $k$  is the reciprocal time,  $s^{-1}$ . The minus sign on the left side of the equation indicates that substance A is disappearing. For first-order reactions the half-life and the time needed to reach completion are independent of the the concentration.

The following reaction is a second-order reaction. Here the rate of the reaction depends on the disappearance of either A or B.



As for the first-order reaction, this relation can be put in differential form as well, which yields:

$$-\frac{dA}{dt} = -\frac{dB}{dt} = k[A][B] \quad (\text{A.4})$$

The differential equation of (A.3) can be put in integrated form and depends on the initial concentrations  $[A]_0$  and  $[B]_0$ . If these are equal the integrated form becomes:

$$kt = \frac{[A]_0 - [A]}{[A]_0[A]} \quad (\text{A.5})$$

If  $[A]_0$  and  $[B]_0$  are not equal then the integrated form becomes.

$$kt = \frac{2.303}{[B]_0 - [A]_0} = \frac{[A]_0[B]}{[B]_0[A]} \quad (\text{A.6})$$

## Appendix B

### Oxidizing agents Ru(bpy)

#### Cerium

Standard electrode potential: 1.61V

(NH)<sub>4</sub>Ce(NO<sub>3</sub>)<sub>6</sub> (orange-red crystals)

(NH)<sub>4</sub>Ce(SO<sub>4</sub>)<sub>4</sub> (orange coloured solid)



#### Lead

Standard electrode potential: 1.69V

Lead(IV)acetate: Pb(C<sub>2</sub>H<sub>3</sub>O<sub>2</sub>)<sub>4</sub>



#### Silver

Standard electrode potential: 1.98V

Ag(II)picolinate



#### Cobalt

Standard electrode potential: 1.82V

Cobalt(III)acetylacetonate



## Appendix C

### Calibration measurements $\text{KMnO}_4$

Similar to Ruthenium bipyridine a calibration curve for potassium permanganate was obtained. Table C.1 shows concentrations in the the seven cuvettes prepared for the experiment. The solutions were prepared from a 1 mM stock solution  $\text{KMnO}_4$ . The cuvettes were placed in UV/vis spectrometer and the absorbance was measured at  $\lambda_{max}$  of 546 nm and at 488 nm.

Cuvette	Concentration in [ $\mu\text{M}$ ]	Absorbance at 546 nm	Absorbance at 488 nm
1	1.000	1.619	1.097
2	0.500	0.863	0.545
3	0.250	0.444	0.277
4	0.100	0.174	0.108
5	0.050	0.089	0.058
6	0.025	0.040	0.024
7	0.001	0.015	0.011

Table C.1: Overview of the concentrations  $\text{KMnO}_4$  in mM of the 1 ml, 1 cm path length cuvettes with the corresponding absorbance (arbitrary units) measured in the spectrometer at 546 and 488 nm.

In figure C.1 the absorbance at 556 nm as a function of time is shown together with the data points and fit. A linear coefficient of  $1.62 \text{ A mM}^{-1}$  was found with  $R^2 = 0.9987$ .

Another calibration curve was made for the absorbance at the wavelength of 488 nm. Here a linear coefficient of  $1.10 \text{ A mM}^{-1}$  was found with  $R^2 = 0.999954$ .

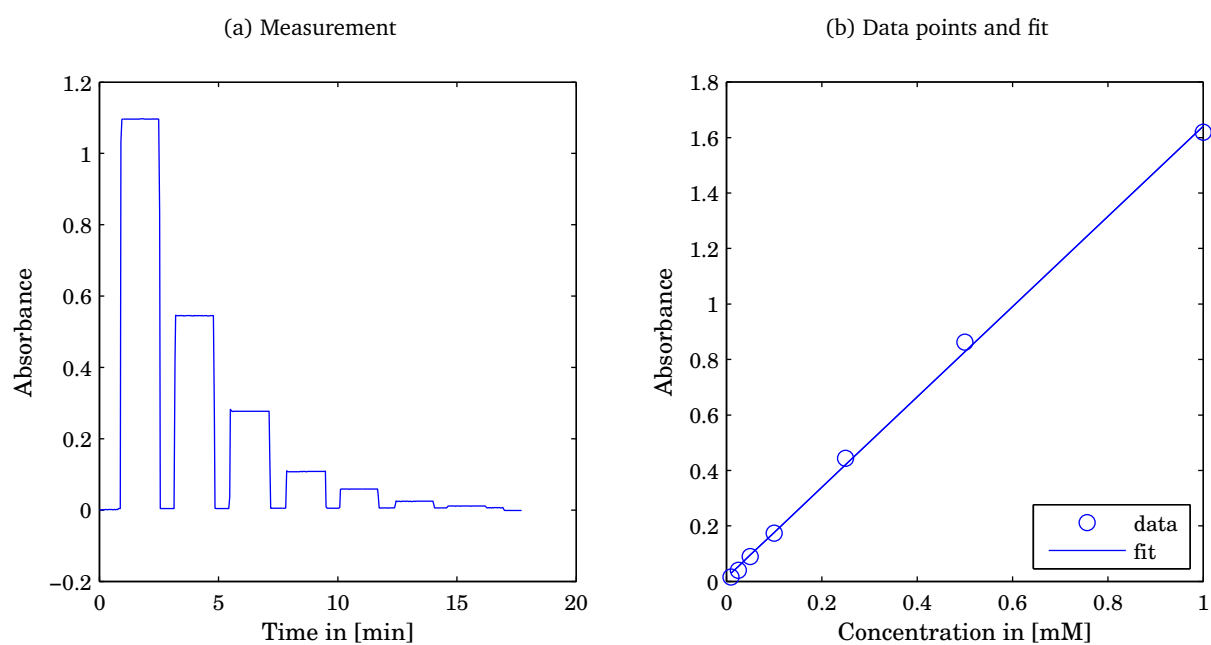


Figure C.1: Calibration measurement for  $[\text{Ru}(\text{bpy})_3]^{2+}$  at the wavelength of 546 nm. C.1a shows the absorbance over time for the seven prepared solutions. C.1b shows the obtained data points together with the datafit, a linear coefficient of  $1.62 \text{ AmM}^{-1}$  with  $R^2 = 0.9987$ .

# Appendix D

## Additional Measurements

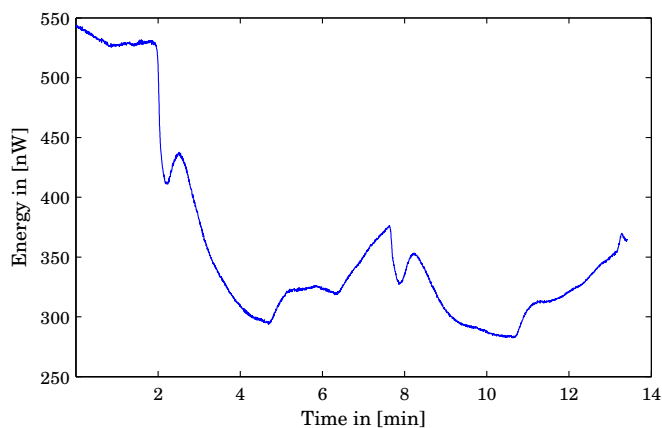


Figure D.1: Alternating H<sub>2</sub>O and Ru(bpy) with an interval of 3 minutes at a flow rate of 4  $\mu$ L/min, the dashed lines indicate switching of the pumps.

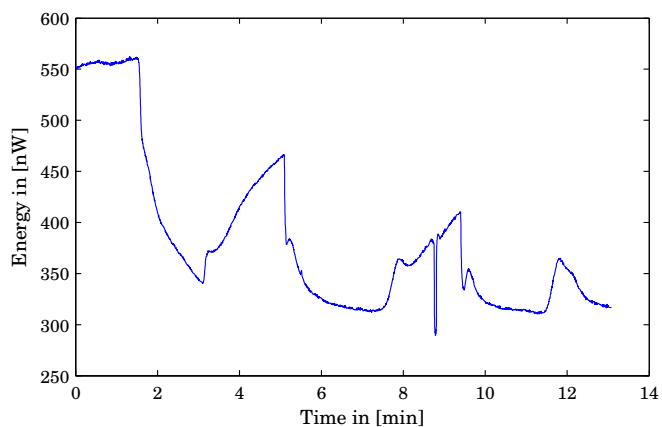


Figure D.2: Alternating H<sub>2</sub>O and Ru(bpy) with an interval of 2 minutes at a flow rate of 20  $\mu$ L/min